Taylor & Francis
Taylor & Francis Group

Spectroscopy Letters

An International Journal for Rapid Communication

ISSN: 0038-7010 (Print) 1532-2289 (Online) Journal homepage: http://www.tandfonline.com/loi/lstl20

High-pressure and high-temperature Raman study of cinnabar

Jianjun Jiang, Heping Li, Chaoshuai Zhao, Shuangming Shan & Pan Wang

To cite this article: Jianjun Jiang, Heping Li, Chaoshuai Zhao, Shuangming Shan & Pan Wang (2017) High-pressure and high-temperature Raman study of cinnabar, Spectroscopy Letters, 50:6, 342-346, DOI: 10.1080/00387010.2017.1331246

To link to this article: https://doi.org/10.1080/00387010.2017.1331246

Accepted author version posted online: 26 May 2017.
Published online: 26 May 2017.

SPECTROSCOPY LETTERS
2017, VOL. 50, NO. 6, 342–346
https://doi.org/10.1080/00387010.2017.1331246

Taylor & Francis
Taylor & Francis Group

High-pressure and high-temperature Raman study of cinnabar

Jianjun Jiang[a,b], Heping Li[a], Chaoshuai Zhao[a,b], Shuangming Shan[a], and Pan Wang[a,b]

[a]Key Laboratory of High Temperature and High Pressure Study of the Earth's Interior, Institute of Geochemistry, Chinese Academy of Sciences, Guizhou Province, China; [b]Graduate School of Chinese Academy of Sciences, Beijing, China

ABSTRACT

The effects of temperature (300–600 K) and pressure (0–31.8 GPa) on the Raman spectra of natural cinnabar powder were investigated in a heatable diamond anvil cell. Raman spectral changes caused by phase transitions were observed at high pressures, which suggests a phase transformation from pure hexagonal to the coexistence of a hexagonal and rock salt structure, and finally to the rock salt structure. With increasing pressure, A_1 and E^2_{TO} modes exhibited a blueshift (0.87 cm^{-1}/GPa) and redshift (−3.64 cm^{-1}/GPa), respectively, while both modes underwent a redshift (−2.22 and -2.09×10^{-2} cm^{-1}/K, respectively) with increasing temperature. The mode Grüneisen parameters of A_1 and E^2_{TO} at room temperature were calculated by the pressure dependences of the vibrational frequencies and the X-ray diffraction data from previous research. Simultaneous high-pressure and high-temperature results were globally fitted, and the coupling coefficients for temperature and pressure dependence of the Raman shifts were determined to be 7.28×10^{-4} and 5.12×10^{-4} cm^{-1}/K · GPa for A_1 and E^2_{TO}, respectively.

ARTICLE HISTORY
Received 27 March 2017
Accepted 12 May 2017

KEYWORDS
Cinnabar; high pressure and high temperature; phase transition; Raman spectroscopy

Introduction

Mercuric sulfide has two crystal structures, the more stable hexagonal (cinnabar) structure and the zinc blend structure.[1,2] The primitive cell of cinnabar is composed of two coaxial helices with three S atoms and three Hg atoms, respectively.[3] As the most common source ore for refining elemental mercury, the pressure-induced cinnabar phase transition from hexagonal to rock salt structure has been widely investigated.[4–7] In an X-ray diffraction study, Huang and Ruoff[5] found that cinnabar transitioned to its rock salt structure at a pressure of ~13 GPa. Later, Fan et al.[4] observed a peak corresponding to the rock salt phase at ~15 GPa, thereby suggesting the coexistence of rock salt and cinnabar structures in the 15–23 GPa range. A discontinuity in the pressure-induced reduction of the electrical conductivity was found at 29 GPa, which seemed to indicate a phase transformation.[8] However, with the X-ray diffraction pattern and Raman spectra combined, Werner et al. suggested no phase transition occurred up to 24 GPa.[6]

To date, to our knowledge, no systematic Raman study of cinnabar has been performed under simultaneous high-pressure and high-temperature conditions. In this work, we measured the Raman spectra of cinnabar up to 31.8 GPa and 600 K, and apparent changes owing to phase transitions were observed. The temperature and pressure dependence of two Raman-active modes, A_1 and E^2_{TO}, were evaluated, and the Grüneisen parameter γ at room temperature was calculated in combination with the pressure dependence of volume of cinnabar.

Experimental

The sample used in this study is naturally occurring single crystal of cinnabar collected from central Guangxi, Southwest China. The results of electron probe microanalysis present in Table 1 support the chemical formula of the crystal as mercuric sulfide in high purity. The X-ray diffraction data proceeding in jade 7.0 indicate that the sample has a hexagonal structure with the following lattice parameters: a = b = 3.165 Å, c = 12.318 Å, and $\alpha = \beta = 90°$, $\gamma = 120°$ (Fig. 1).

In this study, the sample was crushed into powder (~10 micron) and then prepressed into a thin flake (~40 micro in thickness), and finally loaded into a Zha-Bassett-type diamond anvil cell with an external electric resistance heating furnace.[9,10] A few ruby grains were placed in the Re gasket chamber for pressure measurement, and the mixture of methanol, ethanol, and water with the ratio of 16:3:1 was applied as the pressure-transmitting medium. The platinum-rhodium-platinum thermocouple was directly bonded to the diamond using heat conduction glue, and the heating furnaces around the sample cell were externally connected to an OMEGA temperature controller for real-time temperature regulation (regulation accuracy is 1 K). At room pressure, the thermal stage from Instec Inc. (with a mK2000 series high-precision temperature controller, ±0.001 K) was applied to investigate the temperature dependence of Raman spectra of cinnabar. The Spectra Physics 514.5 nm argon ion laser (laser spot size is 5 μm) was used as the excitation light source in combination with a Renishaw inVia micro-confocal laser Raman spectrometer (spectrometer resolution: ±1 cm^{-1}; repetition

CONTACT Heping Li liheping2014@hotmail.com Key Laboratory of High Temperature and High Pressure Study of the Earth's Interior, Institute of Geochemistry, Chinese Academy of Sciences, Guizhou Province, China.
Color versions of one or more of the figures in the article can be found online at www.tandfonline.com/lstl.

Table 1. The chemical composition of the sample analyzed by electron probe microanalysis. (Operating conditions: accelerating voltage 25 kV; specimen current 10 nA).

Atomic constituent	Concentration in cinnabar (wt%)
Sulfur	13.56 (11)
Manganese	0.03 (0)
Copper	0.00 (0)
Iron	0.27 (4)
Nickel	0.04 (1)
Titanium	0.15 (3)
Mercury	86.03 (51)
Tin	0.01 (1)
Lead	0.00 (0)
Antimony	0.05 (1)
Total	100.14 (72)

rate: $\pm 0.2\ cm^{-1}$). In the simultaneous high-temperature and high-pressure experiments, the sample cell load was increased to a certain pressure, the diamond anvils were held fixed, and the temperature was gradually heated up to 600 K at 50 K intervals. The excitation laser powers were typically 40 mW for the Raman spectra and 10 μW for fluorescence. With a 2400 groove/mm grating, the Raman spectra were collected in the ranges of 150–500 cm^{-1} for the cinnabar Raman shift and at 685–720 nm for the ruby fluorescence.

Results and discussion

Raman spectra of cinnabar under high pressure and ambient temperature

At ambient conditions (1 atm. and 300 K), three first-order vibrational modes of the sample, A_1 (255.6 cm^{-1}), E^1_{TO} (284.3 cm^{-1}), and E^2_{TO} (345.8 cm^{-1}), were observed in the frequency range of 150–500 cm^{-1}, which is similar to previously published research.[11–16] The A_1 and E^2_{TO} spectral peaks were very sharp, although the E^1_{TO} presented in low intensity. The diamond anvil cell pressure was increased gradually, and the pressure generated in the sample cell was determined by an online ruby pressure calculator.[17,18] The Raman spectra of cinnabar at high pressure and room temperature are shown in Fig. 2(a).

As shown in Fig. 2(a), the Raman peaks broadened, and the background signal increased as the pressure increased. The E^1_{TO} peak spread more and became unresolvable at higher pressure, and the A_1 and E^2_{TO} peaks broadened, but were still visible up to 24 GPa. With increasing pressure, the A_1 and E^2_{TO} modes exhibited a redshift and blueshift, respectively, and the A_1 mode depended more on pressure than the E^2_{TO} mode; no anomalies were detected up to 20.7 GPa. As the pressure increased, the smooth spectra of cinnabar became rough and an obvious broadening of the A_1 and E^2_{TO} peaks occurred. When the pressure reached 25.5 GPa, the E^2_{TO} peak disappeared and only two broad crests were observed—this state was observed up to a pressure of 31.8 GPa.

The full width at half maximum of the A_1 peak changed slightly when the pressure increased from ambient condition to 14.4 GPa, and then gradually increased with increasing pressure, whereas there was a steep increase in the full width at half maximum of the A_1 band between 20.7 and 22.4 GPa (Fig. 2(b)).

Comprehensive analysis of the pressure dependence of Raman spectra and full width at half maximum in addition to the X-ray diffraction results from Fan et al. suggest the phase boundaries of cinnabar are 15 GPa and 23 GPa. However, based on the Raman spectroscopy experiments, we concluded that there was no phase transition before 20.7 GPa, in accord with the findings of Werner et al., in which there was no sign of transition evidence in Raman spectra at pressures <20 GPa. Nevertheless, a phase transition from cinnabar to the rock salt structure may begin to occur at pressures between 20.7 and 22.4 GPa, as some of the cinnabar structure was transformed into the rock salt structure during this pressure range, which led to a sharp peak widening of the Raman modes. Thus, both phases coexisted in the 22.4–24.7 GPa pressure range, and the remaining Raman peaks of the cinnabar structure possibly came from the residual phase resulting from the sluggishness of the transition at that pressure.[7] Most of the sample changed from cinnabar to the rock salt structure at pressures greater than 25.5 GPa, as indicated by the disappearance of E^2_{TO}. As there was no active optical phonon for the rock salt structure, a smooth Raman spectrum of the pure rock salt structure was not observed at pressures greater than 25.5—there were only two broad crests, which may be

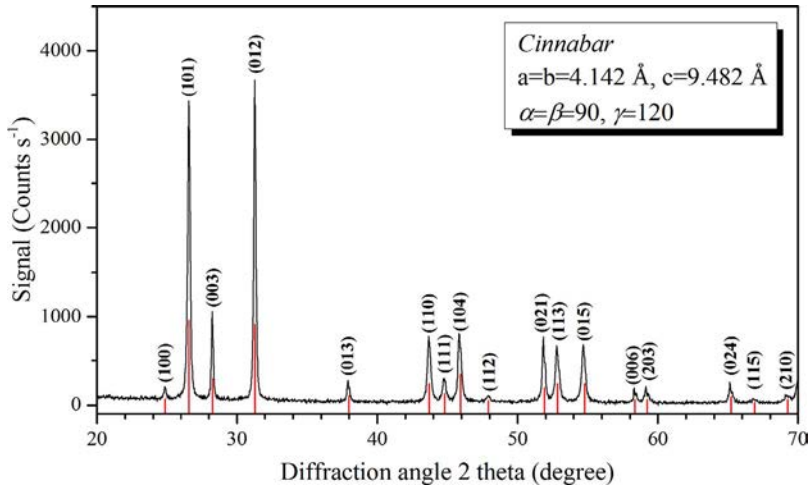

Figure 1. The X-ray diffraction pattern of the sample. (Operating conditions: working voltage 40 kV; working current 40 mA.)

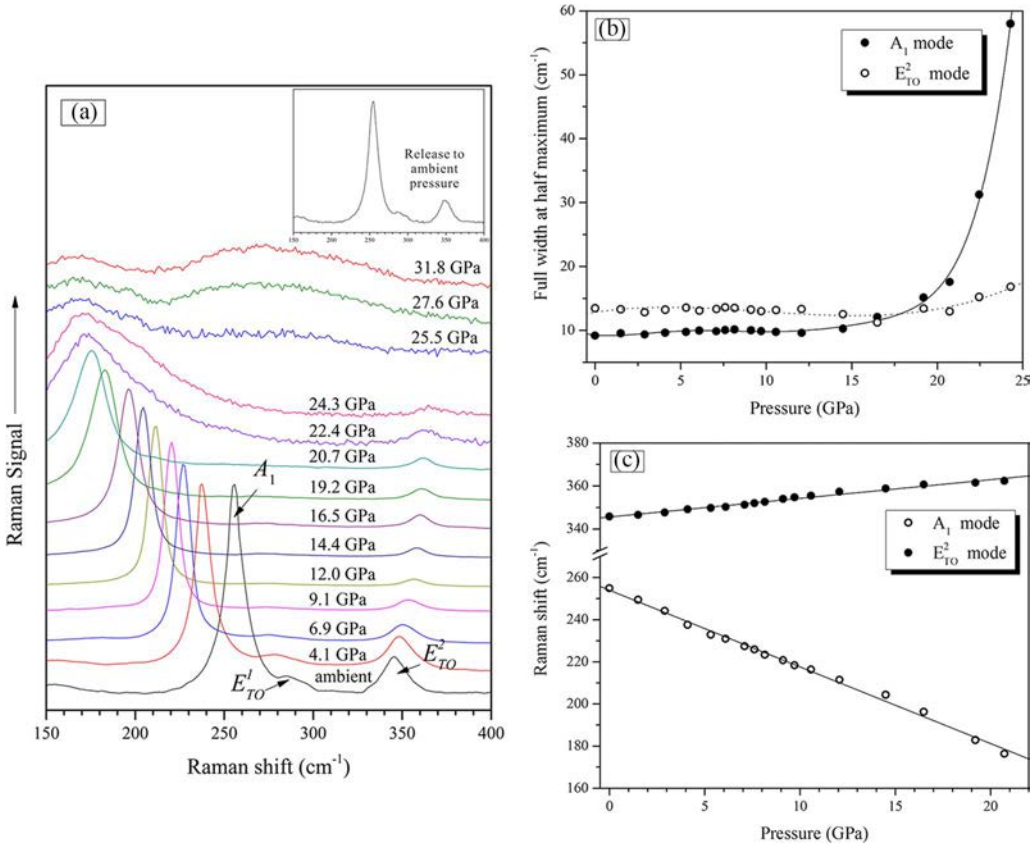

Figure 2. Pressure dependence of (a) Raman spectra, (b) Raman shifts, and (c) full width at half maximum of cinnabar at room temperature. (Operating conditions: excitation laser power 40 mW; grating 2400 groove/mm.)

attributed to amorphization. When we released the pressure in the chamber, the cinnabar Raman spectra recovered and only a slight change in intensity was found, which indicated that the pressure-induced phase change of cinnabar is reversible. The relationship between pressure and Raman shifting of A_1 and E^2_{TO} at pressures less than 20.7 GPa is shown in Fig. 2(c), and can be well fit to linear equations:

$$\begin{cases} \nu(A_1) = 254.0(7) - 3.64(06) \times P & (R^2 = 0.995) \\ \nu(E^2_{TO}) = 345.6(3) + 0.87(03) \times P & (R^2 = 0.983) \end{cases} \quad (1)$$

where ν is wave number in cm^{-1}, and P is pressure in GPa.

The mode Grüneisen constant of cinnabar can be expressed as follows:[19]

$$\gamma_i = -\frac{d\ln\omega_i}{d\ln V} = -\frac{d\ln\omega_i}{dP}\frac{dP}{d\ln V} \quad (2)$$

where γ_i and ω_i are the Grüneisen constant and Raman shift of mode i, respectively. V is the volume of unit cell. The value of $\frac{dP}{d\ln V}$ at ambient temperature can be determined to be −61.66 by the x-ray experiment work was finished by Fan et al. in APS (Advanced Photon Source, USA). Then we can calculate γ_i using the data of our Raman experiment.

$$\gamma_{A_1} = -1.06, \quad \gamma_{E^2_{TO}} = 0.15 \quad (3)$$

We found that mode Grüneisen constant of A_1 is negative and its absolute value is much higher than E^2_{TO}, suggesting that the anharmonicity effect on mode A_1 vibration is larger than on mode E^2_{TO}.

Raman spectra of cinnabar under high temperature and ambient pressure

To date, the temperature dependence of Raman spectra of cinnabar has been investigated only in low temperatures from 70 K to 298 K.[20,21] In this study, the Raman scattering spectra were obtained using the thermal stage up to 600 K (at room pressure). One of the thin flakes (around 0.1 mm) of pre-pressed powder sample was loaded on the heating area of the thermal stage, and the 180° back-scattering Raman signals were collected.

With increasing temperature, the Raman peaks of the samples broadened, and most Raman vibrational modes were gradually masked by noise; however, the A_1 and E^2_{TO} modes were still resolvable. In the range of 300–573 K, the A_1 and E^2_{TO} modes followed a systematic redshift with increasing temperature (Fig. 3). The linear regression results are shown in Eq. [4], where T is the temperature in Kelvin. Both modes showed a normal mode behavior with increasing temperature—that is, negative $\partial\nu/\partial T$ and no sign of instability or discontinuity, which means that cinnabar remained stable over the temperature range of 300–573 K. However, at temperatures higher than 600 K, the sample was burnt at the signal laser spot, and the Raman spectrum had no observable peak.

$$\begin{cases} \nu(A_1) = 261.7(4) - 2.22(10) \times 10^{-2} \times T & (R^2 = 0.976) \\ \nu(E^2_{TO}) = 351.8(5) - 2.09(11) \times 10^{-2} \times T & (R^2 = 0.967) \end{cases} \quad (4)$$

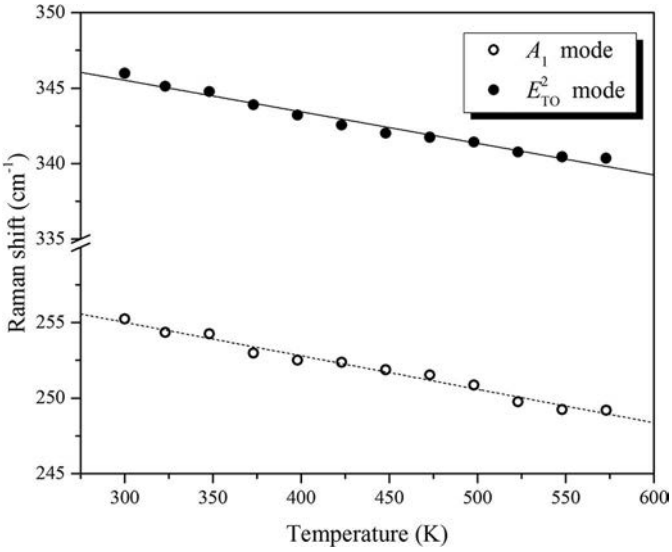

Figure 3. The temperature dependence of Raman modes of cinnabar at ambient pressure.

Raman spectra of cinnabar under simultaneous high pressure and high temperature

The influence of temperature and pressure on the frequency shift of cinnabar has been discussed above. However, the total effect of temperature and pressure on the high-temperature and high-pressure environment is not simply the linear superposition of the two effects, as there may be coupling effects of pressure and temperature on the overall Raman frequency shift.[10] In this work, we fixed the diamond anvil cell at four different pressure values (3.9, 9.4, 12.6, and 16.3 GPa), heated the sample cell up to 600 K, and measured the *in situ* Raman spectra of the sample.

In the heating process, the pressure in the sample cell experiences variations caused by temperature-generated heat expansion of the diamond anvil cell. Therefore, ruby fluorescence spectra at every temperature point were collected for pressure correction. In simultaneous high-temperature and high-pressure condition, the fluorescent shift of ruby gauge will comprehensively be affected by temperature and pressure; however, in the range of 0–20 GPa and 300–600 K, there is weak temperature dependence of the pressure-induced wavelength shift, so the pressure can be calculated after deducting the temperature-induced shift.[22]

$$\begin{cases} \Delta\lambda_{R_T} = -0.00746(4)\Delta T - 3.01(25) \times 10^{-6}\Delta T^2 \\ \qquad\qquad + 8.76(33) \times 10^{-9}\Delta T^3 \\ P = 1884\left(\frac{\Delta\lambda}{\lambda_0}\right)\left[1 + 5.5\left(\frac{\Delta\lambda}{\lambda_0}\right)\right] \end{cases} \tag{5}$$

where $\Delta\lambda_{R_T}$ is temperature-induced fluorescent shift in nm and $\Delta T = T - 300$ is in K. λ_0 is the fluorescent peak at 300 K and $\Delta\lambda = \lambda - \lambda_0$ is the pressure-induced shift of the fluorescent peak (after the deduction of temperature-induced shift $\Delta\lambda_{R_T}$).

The temperature in the sample chamber increased at 25 K intervals to 600 K, and the Raman spectra were collected when the temperature stabilized. The pressure dependence of the Raman shift at different temperatures and the global fitting results of both A_1 and E^2_{TO} modes are shown in Fig. 4(a) and Fig. 4(b), respectively.

The experimental results under high temperature and high pressure were fit to two-variable linear equations using Origin software; the fitting results are shown as Eq. [2]. The pressure and temperature dependence of the A_1 and E^2_{TO} peaks were calculated (Fig. 4(b), the color plane is the global fitting surface).

$$\begin{cases} \nu(A_1) = 262.0(6) - 3.59(6) \times P \\ \qquad\qquad - 2.25(13) \times 10^{-2} \times T \qquad (R^2 = 0.991) \\ \qquad\qquad + 7.28(1.26) \times 10^{-4} \times P \times T \\ \nu(E^2_{TO}) = 351.6(4) + 0.76(4) \times P \\ \qquad\qquad - 2.08(8) \times 10^{-2} \times T \qquad (R^2 = 0.976) \\ \qquad\qquad + 5.12(89) \times 10^{-4} \times P \times T \end{cases} \tag{6}$$

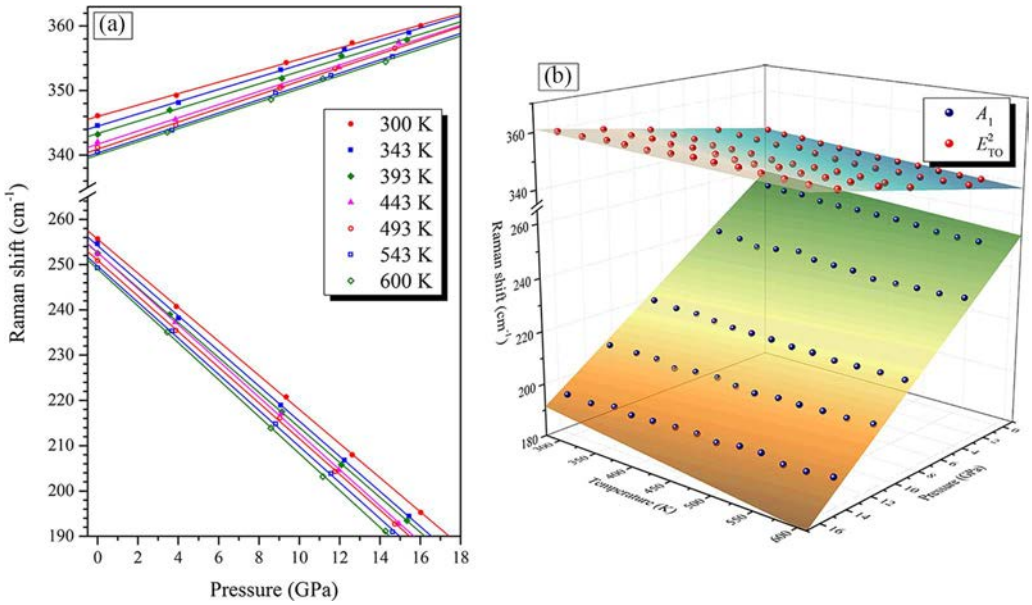

Figure 4. (a) Pressure dependence of the Raman shift at different temperatures and (b) its global fitting surface.

As shown in Eq. [6], the Raman shifts of A_1 and E^2_{TO} displayed a similar dependence on temperature at the rates of $-2.25(13)$ and $-2.08(8) \times 10^{-2}$ cm^{-1}/K, respectively, at ambient pressure. In addition, we obtained coupling coefficients for temperature and pressure, $7.28(1.26) \times 10^{-4}$ and $5.12(89) \times 10^{-4}$ (cm^{-1}/K · GPa), for the A_1 and E^2_{TO} Raman shifts, respectively. This indicated that the effect of temperature on the Raman shift weakens with increasing pressure, and, hence, the effect of temperature on the frequency shift at high pressure is much smaller than at ambient conditions, which can be observed in Fig. 4(b).

Conclusions

In situ Raman scattering measurements of natural cinnabar were conducted under pressure and temperature conditions not exceeding 31.8 GPa and 600 K, respectively. The following conclusions were made.

1. Changes in the Raman spectra caused by pressure-induced phase transition were observed—the hexagonal to rock salt structure transition began at 20.7–22.4 GPa and the two phases coexisted from 22.4 to 24.7 GPa, followed by the disappearance of the hexagonal phase at pressures higher than 25.5 GPa.
2. The A_1 and E^2_{TO} Raman modes of cinnabar had a negative and positive dependence on the pressure, respectively, while they experienced a systematic redshift with increasing temperature.
3. The coupling effect of temperature and pressure on the A_1 and E^2_{TO} Raman shifts were determined by simultaneous high-temperature and high-pressure experiments, which indicated that the redshift effect of temperature on the Raman peaks decreased with increasing pressure.

Acknowledgments

We thank four anonymous reviewers and editor Professor R. G. Michel for their very constructive comments and suggestions in the reviewing process, which helped us greatly in improving the manuscript.

Funding

This work was financially supported by the Strategic Priority Research Program (B) of the Chinese Academy of Sciences (XDB 18010401) and the "135" Program of Institute of Geochemistry of Chinese Academy of Science.

References

[1] Carlson, E. The growth of HgS and $Hg_3S_2Cl_2$ single crystals by a vapor phase method. *Journal of Crystal Growth* **1967**, *1*, 271–277.
[2] Dawson, P. The vibrational spectrum of α-mercuric sulphide. *Spectrochimica Acta Part A: Molecular Spectroscopy* **1972**, *28*, 2305–2310.
[3] Cardona, M.; Kremer, R.; Siegle, G.; Muñoz, A.; Romero, A.; Schmidt, M. Electronic and phononic properties of cinnabar: *Ab initio* calculations and some experimental results. *Physical Review B* **2010**, *82*, 085210.
[4] Fan, D.; Zhou, W.; Liu, C.; Wan, F.; Xing, Y.; Liu, J.; Li, Y.; Xie, H. Phase transition and EOS of cinnabar (α-HgS) at high pressure and high temperature. *Chinese Physics Letters* **2009**, *26*, 046402.
[5] Huang, T.; Ruoff, A. Pressure-induced phase transition of HgS. *Journal of Applied Physics* **1983**, *54*, 5459–5461.
[6] Werner, A.; Hochheimer, H.; Strössner, K.; Jayaraman, A. High-pressure x-ray diffraction studies on HgTe and HgS to 20 GPa. *Physical Review B* **1983**, *28*, 3330.
[7] Huang, T.; Ruoff, A. High-pressure-induced phase transitions of mercury chalcogenides. *Physical Review B* **1985**, *31*, 5976.
[8] Hao, A.; Gao, C.; Li, M.; He, C.; Huang, X.; Zhang, D.; Yu, C.; Liu, H.; Ma, Y.; Tian, Y.; Zou, G. A study of the electrical properties of HgS under high pressure. *Journal of Physics: Condensed Matter* **2007**, *19*, 425222.
[9] Zha, C.; Krasnicki, S.; Meng, Y.; Yan, C.; Lai, J.; Liang, Q.; Mao, H.; Hemley, R. Composite chemical vapor deposition diamond anvils for high-pressure/high-temperature experiments. *High Pressure Research* **2009**, *29*, 317–324.
[10] Jiang, J.; Li, H.; Dai, L.; Hu, H.; Zhao, C. Raman scattering of 2*H*-MoS_2 at simultaneous high temperature and high pressure (up to 600 K and 18.5 GPa). *AIP Advances* **2016**, *6*, 035214.
[11] Gotoshia, S.; Gotoshia, L. Laser Raman and resonance Raman spectroscopies of natural semiconductor mineral cinnabar, α-HgS, from various mines. *Journal of Physics D: Applied Physics* **2008**, *41*, 115406.
[12] Nusimovici, M.; Meskaoui, A. Raman scattering by α-HgS (Cinnabar). *Physica Status Solidi (b)*, **1973**, *58*, 121–125.
[13] Shabunya-Klyachkovskaya, E.; Gaponenko, S.; Vaschenko, S.; Stankevich, V.; Stepina, N.; Matsukovich, A. Plasmon enhancement of Raman scattering by mercury sulfide microcrystals. *Journal of Applied Spectroscopy* **2014**, *81*, 399–403.
[14] Zallen, R.; Lucovsky, G.; Taylor, W.; Pinczuk, A.; Burstein, E. Lattice vibrations in trigonal HgS. *Physical Review B* **1970**, *1*, 4058–4070.
[15] Imaino, W.; Simpson, C.; Becker, W.; Ramdas, A. Resonant Raman effect in cinnabar. *Physical Review B* **1980**, *21*, 634.
[16] Scheuermann, W.; Ritter, G. Raman spectra of cinnabar (HgS), realgar (As_4S_4) and orpiment (As_2S_3). *Zeitschrift für Naturforschung A* **1969**, *24*, 408–411.
[17] Dewaele, A.; Torrent, M.; Loubeyre, P.; Mezouar, M. Compression curves of transition metals in the Mbar range: Experiments and projector augmented-wave calculations. *Physical Review B* **2008**, *78*, 104102.
[18] Rekhi, S.; Dubrovinsky, L.; Saxena, S. Temperature-induced ruby fluorescence shifts up to a pressure of 15 GPa in an externally heated diamond anvil cell. *High Temperatures-high Pressures* **2008**, *31*, 299–305.
[19] Wang, K.; Reeber, R. Mode Grüneisen parameters and negative thermal expansion of cubic ZrW_2O_8 and $ZrMo_2O_8$. *Applied Physics Letters* **2000**, *76*, 2203.
[20] Frost, R.; Martens, W.; Kloprogge, J. Raman spectroscopic study of cinnabar (HgS), realgar (As_4S_4), and orpiment (As_2S_3) at 298 and 77K. *Neues Jahrbuch für Mineralogie - Monatshefte* **2002**, *10*, 469–480.
[21] Peters, M.; McNeil, L.; Dy, K. Resonant Raman scattering in trigonal HgS. *Solid State Communications* **1996**, *97*, 1095–1099.
[22] Datchi, F.; Dewaele, A.; Loubeyre, P.; Letoullec, R.; Le Godec, Y.; Canny, B. Optical pressure sensors for high-pressure–high-temperature studies in a diamond anvil cell. *High Pressure Research* **2007**, *27*, 447–463.